Letters

High-Efficiency Asymmetrically Designed Three-Phase Virtual 48-Pulse Power Supply for Electrolytic Hydrogen

Hanlei Tian, *Graduate Student Member, IEEE*, Haoran Cui, Wei Han, *Member, IEEE*, Jagabar Sathik M, *Senior Member, IEEE*, Guozhuang Liang, *Member, IEEE*, Maolin Chen, *Graduate Student Member, IEEE*, and Saad Mekhilef, *Fellow, IEEE*

***Abstract*—To address the low-voltage, high-current requirements in hydrogen production applications, a virtual 48-pulse three-phase rectifier is proposed, and achieves the equivalent performance of four parallel 12-pulse rectifiers (12-PR). The proposed approach builds upon the conventional 12-PR design and incorporates novel asymmetric current injection units (ACIU). The ACIU is installed on the dc side of the ac–dc converter, generating a specific current at the dc link to modulate and enhance the operating modes of the 12-PR. Consequently, the 12-pulse is extended to 48, resulting in an almost sinusoidal input current with a total harmonic distortion of 3.2% and an output current with a ripple rate of 2.3%, thus significantly improving power quality. Furthermore, the asymmetric design of the current injection units eliminates the need for a phase-shifting transformer. The efficacy of the proposed rectifier for electrolytic hydrogen production is validated using a 2.2-kW experimental prototype.**

***Index Terms*—Electrolytic hydrogen production, power quality, renewable energy, three-phase.**

Received 31 December 2024; revised 26 February 2025; accepted 11 March 2025. Date of publication 17 March 2025; date of current version 26 May 2025. This work was supported in part by Guangdong Basic and Applied Basic Research Fund under Grant 2025A1515012012 and in part by the Guangzhou-HKUST(GZ) Joint Funding Program under Grant 2024A03J0680. *(Corresponding author: Wei Han.)*

Hanlei Tian is with the Sustainable Energy and Environment Thrust, The Hong Kong University of Science and Technology (GZ), Guangzhou 511453, China (e-mail: thledu@ieee.org).

Haoran Cui and Guozhuang Liang are with the Electrical Engineering School of Hebei University of Science and Technology, Shijiazhuang 050091, China.

Jagabar Sathik M is with the Faculty of Engineering and Technology, SRM Institute of Science and Technology, Kattankulathur 603203, India (e-mail: mjsathik@ieee.org).

Maolin Chen is with the College of Electrical Engineering, Sichuan University, Chengdu 610065, China (e-mail: chenml@alu.scu.edu.cn).

Saad Mekhilef is with the School of Science, Computing and Engineering Technologies, Swinburne University of Technology, Melbourne, VIC 3122, Australia (e-mail: smekhilef@swin.edu.au).

Wei Han is with the Sustainable Energy and Environment Thrust, The Hong Kong University of Science and Technology (GZ), Guangzhou 511453, China, and also with the Department of Electronic and Computer Engineering, The Hong Kong University of Science and Technology, Hong Kong (e-mail: weihan@hkust-gz.edu.cn).

Color versions of one or more figures in this article are available at https://doi.org/10.1109/TPEL.2025.3552068.

Digital Object Identifier 10.1109/TPEL.2025.3552068

I. Introduction

HYDROGEN energy has become a significant element in the global energy transition due to its high energy density, and its environmental advantages [1]. Various methods exist for hydrogen production, such as water electrolysis, biological processes, photolysis, and fossil fuel reforming. Among these, hydrogen production through renewable energy-powered electrolysis stands out for its ability to produce clean hydrogen while also addressing the issues related to the intermittent and unpredictable nature of renewable energy sources [2]. However, the power conversion systems for electrolysis face critical challenges in balancing harmonic suppression, efficiency, and scalability.

Hydrogen production power sources can generally be classified into two categories. The first is high-frequency pulsewidth modulation (PWM) rectifiers. These systems utilize active switches (e.g., IGBTs) to achieve low input harmonics [<5% total harmonic distortion (THD)] and output ripples through high-frequency modulation [3]. While effective for small-scale applications, their reliance on expensive high-current switching devices becomes cost-prohibitive for MW-scale electrolysis plants. The second is multipulse diodes rectifiers. As the dominant solution for high-power scenarios, these topologies are classified by their pulse configurations. For 12/24-pulse systems, the baseline topology employs phase-shifting transformers to cancel 5th/7th harmonics, yet input current THD remains above 10% [4], failing IEEE 519 standards. Increasing pulse counts to 24 via passive current injection [6], [7] reduces THD to 8%, but introduces auxiliary diode losses and output ripple tradeoffs. For 48-pulse and beyond, recent advances focus on harmonic suppression circuits. Unconventional interphase reactors (UIRs) in [8] achieve 48-pulse operation with THD ≈3.8%, but require complex magnetic designs and suffer from switch-induced losses. Pulse-doubling IPR configurations in [9] and [10] eliminate active components through series/parallel PD-IPR, yet induce substantial conduction losses in high-current paths. Passive voltage harmonic injection in [11] extends pulse to 30 but necessitates bulky series inductors, increasing system volume and cost by 20%. Also, current injection units in [12] enables N-pulse operation via specialized phase-shifting

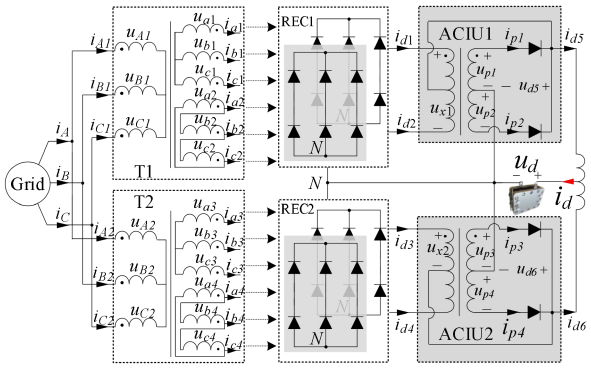

Fig. 1. Main circuit of proposed virtual 48-pulse rectifier.

transformers, but at the expense of component redundancy and control complexity.

While current topological evolution demonstrates progressive harmonic mitigation capabilities, three fundamental constraints are revealed.

1) Pulse multiplication necessitates either multiwinding transformer configurations (increasing magnetic complexity) or lossy auxiliary power stages.
2) Inherent efficiency penalties exceeding 5% power loss (as documented in [9], [10], and [11]) directly conflict with the >95% efficiency mandates for MW-class electrolyzers.
3) Practical scalability remains fundamentally constrained by geometric cost-volume scaling laws proportional to pulse count elevation.

To address these limitations, this letter proposes a 48-pulse hydrogen production power supply based on asymmetric current injection units (ACIUs). The parallel connection of ACIU with the load enables the proposed system to achieve low diode conduction losses. Furthermore, transformers T1 and T2 implement identical winding structures with only output voltage differentiation, significantly simplifying the circuit configuration compared to existing designs. Notably, the ACIUs demonstrate exceptional compactness, contributing merely 1.6% (diode loss proportion) and 1% (volumetric/cost allocation) to the total system implementation. Experimental verification confirms the design's effectiveness with THD maintained below 4% across 20%–100% loading conditions while achieving 98.1% peak efficiency.

II. Proposed Virtual 48-Pulse Method and Working Principle

A. Configuration Analysis of Proposed Method

The proposed parallel topology comprises two Y-Y-D transformers (T1 and T2), two sets of three-phase diode-bridge rectifiers (REC1 and REC2), and two ACIUs (ACIU1 and ACIU2), as illustrated in Fig. 1. It is noteworthy that the asymmetric design of the ACIU eliminates the possibility of phase shifting between T1 and T2.

The ACIU1 and the ACIU2 double the pulse number of the REC1 and the REC2 to 24 through the respective secondary-side diode-bridge circuits, ultimately achieves a 48-pulse output

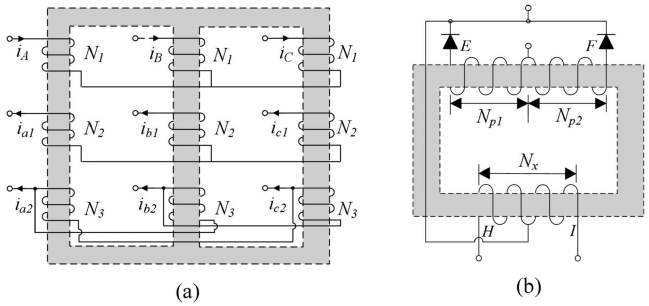

Fig. 2. Winding design of (a) Y-Y-D phase-shifting transformer and (b) ACIU.

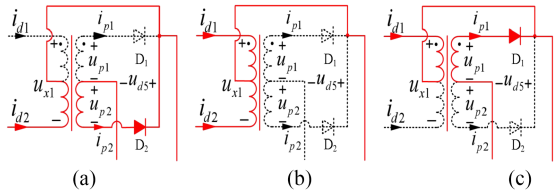

Fig. 3. Working modes of ACIU. (a) Mode I. (b) Mode II. (c) Mode III.

through a parallel connection with a balanced reactor. In addition, Fig. 2(a) shows the winding configuration of the transformer T1&T2. Similarly, Fig. 2(b) shows the winding configuration of the injection transformer. In Fig. 2(a), the turn ratio of the primary and secondary windings of the Y-Y-D phase-shifting transformer meets (1). Also, in Fig. 2(b), N_x, N_{p1}, and N_{p2} are the number of turns, and meet (2)

$$N_1 : N_2 : N_3 = 1 : k_{1,2} : \sqrt{3}k_{1,2} \tag{1}$$

$$N_{p1} : N_{p2} : N_x = m_{1,2} : m_{1,2} : 1 \tag{2}$$

where k_1 and k_2 are the turns ratio between the primary and secondary winding of the transformer T1 and T2, respectively.

B. Operating Modes of ACIU

Owing to the presence of the balanced reactor, both ACIU1 and ACIU2 can operate independently. Given the spatial limitations of this section, the analysis will focus solely on the operational mode of ACIU1. For simplicity, ACIU1's operation is classified into three modes accordance with the relationship between the voltages u_{p1} and u_{d5}, as presented in Fig. 3.

Mode I: When $-u_{p1} > u_{d5}$, the auxiliary diode D_1 is reverse biased, and the auxiliary diode D_2 conducts. The circuit operates as shown in Fig. 3(a). According to the Kirchhoff voltage law (KVL) and Kirchhoff current law, the input current and output voltage of ACIU1 satisfy

$$\begin{cases} i_{d1} = 0 \\ i_{d2} = \frac{2m_1}{2m_1+1} I_{d5} \end{cases} \qquad \begin{cases} i_{p1} = 0 \\ i_{p2} = \frac{1}{2m_1+1} I_{d5} \end{cases}$$

$$\begin{cases} u_{d5} = \frac{2m_1}{2m_1+1} u_{d2} \\ u_{d1} = \frac{2m_1-1}{2m_1+1} u_{d2} \end{cases} . \tag{3}$$

Mode II: When $|u_{p1}| < u_{d5}$, the auxiliary diodes are all reverse biased. The working mode of the circuit is presented in Fig. 3(b).

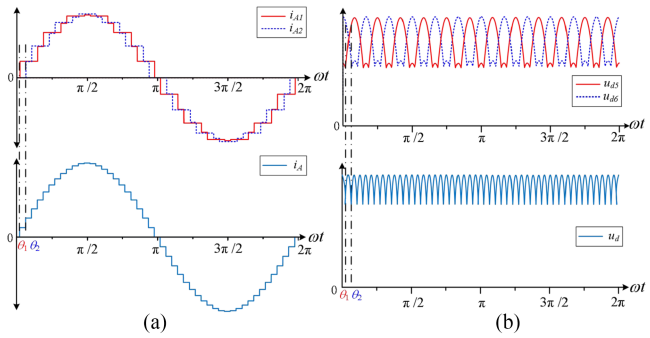

Fig. 4. Principle of pulse wave multiplication of (a) input current and (b) output voltage.

Similarly, the input current and output voltage of ACIU1 meet

$$i_{d1} = i_{d2} = \frac{I_{d5}}{2} \quad i_{p1} = i_{p2} = 0 \quad u_{d5} = \frac{u_{d1} + u_{d2}}{2}. \tag{4}$$

Mode III: When $u_{p1} > u_{d5}$, the auxiliary diode D_2 is reverse biased, and the auxiliary diode D_1 conducts, as shown in Fig. 3(c). Hence, the input current and output voltage of ACIU1 satisfy

$$\begin{cases} i_{d1} = \frac{2m_1}{2m_1+1} I_{d5} \\ i_{d2} = 0 \end{cases} \qquad \begin{cases} i_{p1} = \frac{1}{2m_1+1} I_{d5} \\ i_{p2} = 0 \end{cases}$$

$$\begin{cases} u_{d5} = \frac{2m_1}{2m_1+1} u_{d1} \\ u_{d2} = \frac{2m_1-1}{2m_1+1} u_{d1} \end{cases} \tag{5}$$

where u_{d1}, u_{d2}, and I_{d5} represent the output voltage of rectifier bridge REC1 and the output current of ACIU1, respectively. Also, the relationship with the output current meets

$$I_{d5} = I_{d6} = \frac{I_d}{2}. \tag{6}$$

C. Design Considerations of ACIU

Fig. 4 shows the theoretical waveform of proposed method. It presents an increase in the input current i_A and output voltage u_d to 48-pulse due to the ACIU.

From Fig. 4(a), it is noticed that the input current i_A of the proposed hydrogen production power supply is 48-step. Then, the angle of θ_1 and θ_2 can be expressed as

$$\theta_1 = \frac{-\arctan\left[(2\sqrt{3}-4)m_1 + 2 + \sqrt{3}\right]}{2m_1+1} = \frac{\pi}{48}$$
$$\theta_2 = \frac{-\arctan\left[(2\sqrt{3}-4)m_2 + 2 + \sqrt{3}\right]}{2m_2+1} = \frac{3\pi}{48} \tag{7}$$

where θ_1 and θ_2 are the angle when the working modes of ACIU1 and ACIU2 change for the first time in one cycle.

And, it can be expressed as

$$\theta_{1,2} = \frac{-\arctan(2\sqrt{3}m_{1,2} - 4m_{1,2} + 2 + \sqrt{3})}{2m_{1,2}+1}. \tag{8}$$

According to (7) and (8), the turn ratios of the winding m_1 and m_2 are as

$$m_1 = -\frac{\tan\left(\frac{\pi}{48}\right) + 2 + \sqrt{3}}{2\tan\left(\frac{\pi}{48}\right) + 2\sqrt{3} - 4} \approx 9.4$$
$$m_2 = -\frac{tan\left(\frac{\pi}{16}\right) + 2 + \sqrt{3}}{2tan\left(\frac{\pi}{16}\right) + 2\sqrt{3} - 4} \approx 28.5. \tag{9}$$

The output voltages u_{d5} and u_{d6} of ACIU1 and ACIU2 are different due to the turn ratios, which leads to improper functioning of the interphase reactor. To solve the issues of the above-mentioned analysis, the turn ratio of the transformers T1 and T2 needs to be redesigned. According to KVL, the output voltages u_{d5} and u_{d6} of ACIU1 and ACIU2 are expressed as

$$u_{d5,6} = k_{1,2}U_m \begin{cases} \frac{2\sqrt{3}m_{1,2}}{2m_{1,2}+1}\cos(\omega t) & 0 < \omega t < \theta_{1,2} \\ \frac{\sqrt{3}[(2+\sqrt{3})\cos(\omega t)+\sin(\omega t)]}{4} & \theta_{1,2} < \omega t < \frac{\pi}{6} - \theta_{1,2} \\ \frac{2\sqrt{3}m_{1,2}}{2m_{1,2}+1}\sin\left(\omega t + \frac{\pi}{3}\right) & \frac{\pi}{6} - \theta_{1,2} < \omega t < \frac{\pi}{6} \end{cases} \tag{10}$$

where U_m is the amplitude of the input phase voltage.

From (9) and (10), when the rms of u_{d5} and u_{d6} are the same, k_1 and k_2 needs to meet

$$k_2 : k_1 = 0.983 : 1. \tag{11}$$

III. Performance Analysis of ACIU

A. THD Analysis of Input Current

Based on the analysis of the operating modes, the input current i_A is obtained in (12) shown at the bottom of the next page. Consequently, using (9), (11), and (12), the THD of the input current is calculated to be 3.8%

B. Capacity Analysis of ACIU

According to the mode analysis of ACIU, the input voltages of ACIU1 and ACIU2 can be calculated as follows:

$$u_{x1,2} = \begin{cases} \frac{2\sqrt{3}k_{1,2}U_m}{2m_{1,2}+1}\cos(\omega t), & \omega t \in \left[0, \theta_{1,2}\right) \\ \sqrt{3}k_{1,2}U_m\left(\cos(\omega t) \right. \\ \quad \left. - \sin\left(\omega t + \frac{\pi}{3}\right)\right), & \omega t \in \left[\theta_{1,2}, \frac{\pi}{6} - \theta_{1,2}\right) \\ -\frac{2\sqrt{3}k_{1,2}U_m}{2m_{1,2}+1}\sin\left(\omega t + \frac{\pi}{3}\right), & \omega t \in \left[\frac{\pi}{6} - \theta_{1,2}, \frac{\pi}{6}\right) \end{cases} \tag{13}$$

From (13), the rms of the voltage u_{x1} and u_{x2} can be calculated as

$$U_{x1\_rms} = 0.075U_d \qquad U_{x2\_rms} = 0.032U_d. \tag{14}$$

Similarly, the input currents i_{d1} and i_{d3} of ACIU1 and ACIU2 are calculated as follows:

$$i_{d1,3}=\begin{cases}\frac{m_{1,2}}{2m_{1,2}+1}I_d, & \omega t\in\left[0,\theta_1\right)\cup\left[\frac{\pi}{3}-\theta_1,\frac{\pi}{3}\right]\\ \frac{1}{4}I_d, & \omega t\in\left[\theta_1,\frac{\pi}{6}-\theta_1\right)\cup\left[\frac{\pi}{6}+\theta_1,\frac{\pi}{3}-\theta_1\right)\\ 0, & \omega t\in\left[\frac{\pi}{6}-\theta_1,\frac{\pi}{6}+\theta_1\right)\end{cases}. \tag{15}$$

From (15), the rms of the current i_{d1} and i_{d3} are as

$$I_{d1\_\mathrm{rms}}=I_{d2\_\mathrm{rms}}=0.274I_d\quad I_{d3\_rms}=I_{d4\_\mathrm{rms}}=0.326I_d. \tag{16}$$

Similarly, the output currents of ACIU1 and ACIU2 i_{p1} and i_{p3} are calculated as follows:

$$i_{p1,3}=\begin{cases}\frac{1}{4m_1+2}I_d, & \omega t\in\left[0,\theta_{1,2}\right)\cup\left[\frac{\pi}{3}-\theta_{1,2},\frac{\pi}{3}\right)\\ 0, & \omega t\in\left[\theta_{1,2},\frac{\pi}{3}-\theta_{1,2}\right)\end{cases}. \tag{17}$$

From (17), the rms of the currents i_{p1} and i_{p3} are as

$$I_{p1\_\mathrm{rms}}=I_{p2\_\mathrm{rms}}=0.009I_d\quad I_{p3\_\mathrm{rms}}=I_{p4\_\mathrm{rms}}=0.005I_d. \tag{18}$$

Hence, the kVA rating of ACIU1 and ACIU2 are obtained by

$$S_{\mathrm{ACIU1}}=\frac{1}{2}\left[\frac{1}{2}U_{x1\_\mathrm{rms}}I_{d1\_\mathrm{rms}}+\frac{1}{2}U_{x1\_\mathrm{rms}}I_{d2\_\mathrm{rms}}+m_1U_{x1\_\mathrm{rms}}I_{p1\_\mathrm{rms}}+m_1U_{x1\_\mathrm{rms}}I_{p2\_\mathrm{rms}}\right]=1.6\% \tag{19}$$

$$S_{\mathrm{ACIU2}}=\frac{1}{2}\left[\frac{1}{2}U_{x2\_\mathrm{rms}}I_{d3\_\mathrm{rms}}+\frac{1}{2}U_{x2\_\mathrm{rms}}I_{d4\_\mathrm{rms}}+m_1U_{x2\_\mathrm{rms}}I_{p3\_\mathrm{rms}}+m_1U_{x2\_\mathrm{rms}}I_{p4\_\mathrm{rms}}\right]=1\%. \tag{20}$$

IV. Performance Analysis

A. Loss Analysis

The proposed scheme uses a traditional 12 pulse rectifier as the front-end, so its loss calculation will not be repeated. The losses in ACIU mainly consist of the conduction losses of power devices, as well as the core and ohmic losses of the interphase reactor.

1) Conduction Loss of Diodes D_1–D_4*:* Combined with (17), the effective value of the current flowing through diode D_1 can

$$i_A=\begin{cases}0, & \omega t\in\left[0,\theta_1\right)\\ k_1\frac{1}{4\sqrt{3}}I_d, & \omega t\in\left[\theta_1,\theta_2\right)\\ k_1\frac{1}{4\sqrt{3}}I_d+k_2\frac{1}{4\sqrt{3}}I_d, & \omega t\in\left[\theta_2,\frac{\pi}{6}-\theta_2\right)\\ k_1\frac{1}{4\sqrt{3}}I_d+k_2\frac{m_2}{\sqrt{3}(2m_2+1)}I_d, & \omega t\in\left[\frac{\pi}{6}-\theta_2,\frac{\pi}{6}-\theta_1\right)\\ k_1\frac{m_1}{\sqrt{3}(2m_1+1)}I_d+k_2\frac{m_2}{\sqrt{3}(2m_2+1)}I_d, & \omega t\in\left[\frac{\pi}{6}-\theta_1,\frac{\pi}{6}+\theta_1\right)\\ k_1\left(\frac{1}{4}+\frac{1}{4\sqrt{3}}\right)I_d+k_2\frac{m_2}{\sqrt{3}(2m_2+1)}I_d, & \omega t\in\left[\frac{\pi}{6}+\theta_1,\frac{\pi}{6}+\theta_2\right)\\ k_1(\frac{1}{4}+\frac{1}{4\sqrt{3}})I_d+k_2(\frac{1}{4}+\frac{1}{4\sqrt{3}})I_d, & \omega t\in\left[\frac{\pi}{6}+\theta_2,\frac{\pi}{3}-\theta_2\right)\\ k_1\left(\frac{1}{4}+\frac{1}{4\sqrt{3}}\right)I_d+k_2\frac{m_2}{(2m_2+1)}I_d, & \omega t\in\left[\frac{\pi}{3}-\theta_2,\frac{\pi}{3}-\theta_1\right)\\ k_1\frac{m_1}{(2m_1+1)}I_d+k_2\frac{m_2}{(2m_2+1)}I_d, & \omega t\in\left[\frac{\pi}{3}-\theta_1,\frac{\pi}{3}+\theta_1\right)\\ k_1\left(\frac{1}{4}+\frac{1}{2\sqrt{3}}\right)I_d+k_2\frac{m_2}{(2m_2+1)}I_d, & \omega t\in\left[\frac{\pi}{3}+\theta_1,\frac{\pi}{3}+\theta_2\right)\\ k_1\left(\frac{1}{4}+\frac{1}{2\sqrt{3}}\right)I_d+k_2\left(\frac{1}{4}+\frac{1}{2\sqrt{3}}\right)I_d, & \omega t\in\left[\frac{\pi}{3}+\theta_2,\frac{\pi}{2}-\theta_2\right)\\ k_1\left(\frac{1}{4}+\frac{1}{2\sqrt{3}}\right)I_d+k_2\frac{2m_2}{\sqrt{3}(2m_2+1)}I_d, & \omega t\in\left[\frac{\pi}{2}-\theta_2,\frac{\pi}{2}-\theta_1\right)\\ k_1\frac{2m_1}{\sqrt{3}(2m_1+1)}I_d+k_2\frac{2m_2}{\sqrt{3}(2m_2+1)}I_d, & \omega t\in\left[\frac{\pi}{2}-\theta_1,\frac{\pi}{2}\right)\end{cases} \tag{12}$$

TABLE I
COMPARISON RESULTS BETWEEN PROPOSED METHOD AND SIMILAR WORKS

Indicators		Conventional 48-pulse method	Proposed in [8]	Proposed in [9]	Proposed in [10]	Proposed in [13]	Proposed method
THD of input current		≈3.3%	3.81%	3.03%	–	3.556%	3.2%
Passive or active control in PMU		/	Active	Passive	Passive	Passive	Passive
Isolated or not		Yes	No	No	Yes	Yes	Yes
Efficiency of system		≈95%	97.3%	98.2%	96.2%	–	98.1%
Power density		<3W/in³	–	4 A/mm²	–	<4W/in³	6W/in³
Design complexity		Simple	Hard	Medium	Medium	Medium	Simple
Harmonic suppression method		/	Current injection	Current injection	Current injection	Current injection	Current injection
Number of component or unit	Pulse multiplication unit	0	1	3	2	2	2
	Output side diode/switch	48 (main)	12 (main) 6 (series) 4 (parallel)	24 (main) 2 (series) 4 (parallel)	24 (main) 4 (series) 4 (parallel)	24 (main) 2 (series)	24 (main) 4 (parallel)
Transformer design	Connection type	Zig-zag-delta-wye	Delta-connected	Polygon-connected	Double delta-wye-wye	Wye-Zig-zag-Wye	Wye- wye- delta
	Number of *m*	4	2	3	2	1	1
Overall magnetic ratings		>220%	–	31.575%	145.9%	>150%	127%
Application scenarios		Low, medium and high voltage, high power	Medium and high voltage, high power	Low and medium voltage, high power	Medium and high voltage, high power	Medium and high voltage, high power	Electrolysis, and other low voltage, high current

Note: *m* is the transformer except for conventional or improved interphase reactor. - represents no-data. / indicates that the technology has not been adopted.

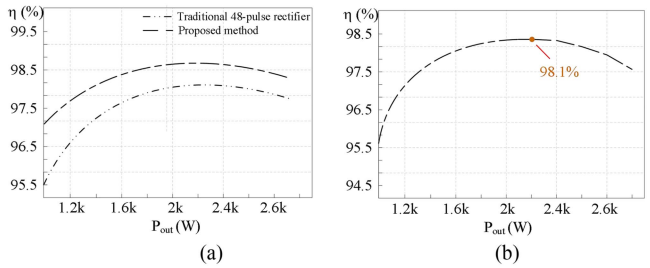

Fig. 5. Efficiency curve under different output power (a) of simulation results and (b) experimental results.

be expressed as

$$I_{D1\_\mathrm{rms}} = \sqrt{\frac{1}{2\pi}\int_0^{2\pi} {i_{p1}}^2 d\omega t} = 0.009 I_d. \tag{21}$$

The total conduction loss of diodes D_1–D_2 is

$$P_{\mathrm{loss}\_D1-D2} = 2 \times 0.009 I_d \times V_{\mathrm{on}} = 0.018 I_d V_{\mathrm{on}} \tag{22}$$

where V_{on} is the conductance voltage drop.

Similarly, the effective value of the current flowing through diode D_3 is

$$I_{D3\_\mathrm{rms}} = \sqrt{\frac{1}{2\pi}\int_0^{2\pi} {i_{p3}}^2 d\omega t} = 0.005 I_d. \tag{23}$$

The total conduction loss of diodes D_3–D_4 is

$$P_{\mathrm{loss}\_D3-D4} = 2 \times 0.005 I_d \times V_{\mathrm{on}} = 0.01 I_d V_{\mathrm{on}}. \tag{24}$$

2) Analysis of Interphase Reactor Losses: The losses in the interphase reactor are primarily divided into the core loss and the ohmic loss. Specifically, the core loss can be further categorized into the hysteresis loss P_h and the eddy current loss P_e

$$\begin{cases} P_{h1,2} = m_{1,2} k_{h1,2} f B_{m1,2}^{1.6} \\ P_{e1,2} = m_{1,2} k_{e1,2} f^2 B_{m1,2}^2 \end{cases} \tag{25}$$

where m_1 *and* m_2 is the weight of the interphase reactor, $k_{h1,2}$ and $k_{e1,2}$ denote the iron loss coefficients, f is the operating frequency, and $B_{m1,2}$ is the maximum magnetic flux density.

The ohmic loss of the ACIU1 and ACIU2 can be expressed as follows:

$$P_{o1,2} = I_{d1,3\_\mathrm{rms}}^2 R_{HI1,2} + I_{p1,3\_\mathrm{rms}}^2 R_{EF1,2} \tag{26}$$

where $I_{d1,3\_\mathrm{rms}}$ and $I_{p1,3\_\mathrm{rms}}$ respectively represent the effective values of the primary and secondary side current in ACIU1 and ACIU2. $R_{EF1,2}$, $R_{HI1,2}$ are the winding resistance of ACIU1 and ACIU2, as shown in Fig. 2(b).

To verify the efficiency at various output voltages under rated power and different output power levels, we employed a PSIM-based thermal simulation, with the results displayed in Fig. 5(a). Compared to traditional 48-pulse rectifier, the proposed method significantly reduces the number of phase-shifting transformers and power devices, as shown in Table I, resulting in better efficiency. It is worth noting that the loss of PCB is not considered in the PSIM model, so the simulation efficiency is slightly higher than the measured efficiency, as shown in Fig. 5(b). As seen in Fig. 5, the efficiency for output power ranging from 1.2 to 2.6 kW is also satisfactorily high, at above 95.5%.

B. Comparative Analysis With Similar 48-Pulse Methods

Based on the principle of fairness and to highlight the advantages and limitations of the proposed method, Table I provides a comparison with related studies referenced in [8], [9], [10], and [13]. Furthermore, Table II outlines the costs of different 1MVA rectifiers used for electrolytic hydrogen production. These costs

TABLE II
COST OF DIFFERENT RECTIFIERS

Method (200V/5000A, 1MW)	M1	M2	M3
Transformer	$30,000	$20,000	$20,500
Power switching/diode device	$7,200	$17,000	$2,900
Capacitor and inductor	$1,100	$6,000	$1,100
Control, sensor, and driver	$1,500	$5,000	$1,000
Total	$39,800	$48,000	$25,500

Note: M1 is conventional 48-pulse rectifier achieved by cascading 12-pulse rectifiers. M2 is PWM rectifier proposed in [14]. M3 is the proposed method.

are based on a specific estimation example and should be considered as approximate values.

From the perspective of the efficiency, achieving the simplicity of the pulse multiplication circuit and providing more operating modes in the rectifier necessitates the direct connection of power devices to the load. However, hydrogen production requires electrical energy characterized by low voltage and high current. In comparison to the configuration with six devices in [8] and four devices in [10], the approach presented in this letter utilizes zero devices. As a result, the conduction losses are minimized, and transmission efficiency is improved. Although the quantity is similar, the complex multiport structure in [9] presents a challenge for large-scale production.

From the design complexity, the complexity of the rectifier structure is primarily determined by the phase-shifting transformers and the pulse multiplication unit. Compared to [8] and [13], which employ multiple pulse multiplication circuits and multiwinding phase-shifting transformers to achieve 48-pulse, the components used by the proposed method are all standard parts, such as phase-shifting transformers and pulse multiplication units. Therefore, the manufacturing process is simple and easy to mass produce, and the power density is higher.

From the perspective of the cost, the rectifier's dc output voltage is 200 V, and the current is 5000 A. While comparing the total costs of M1 and M2, the proposed method M3 offers savings of approximately 47% and 77%, respectively. It is important to note that these costs will increase as the nominal power rating rises. In addition, while the base failure rate of diodes is less than 22 Failure in Time (FIT), the IGBT's failure rate is 100 FIT, as reported in [15].

V. RESULT AND DISCUSSION

A 2.2-kW proof-of-concept hardware prototype is built to verify the correctness of the theoretical analysis, as depicted in Fig. 6. A 3-Ω resistor is connected in series with the electrolyzer cell (EC) to facilitate voltage division. In addition, the input voltage of 380 VAC and the bus frequency of 50 Hz are maintained by the power grid simulator 61 815. The turns ratio of ACIU1 is 0.5:0.5:9.4:9.4. The turns ratio of ACIU2 is 0.5:0.5:28.5:28.5. Besides, the experimental parameters employed are consistent with those used in the simulation, where the simulation results is obtained by using PSIM software.

First, the power quality analysis is discussed as follows. Under the same input voltage and power, Fig. 7 illustrates the input

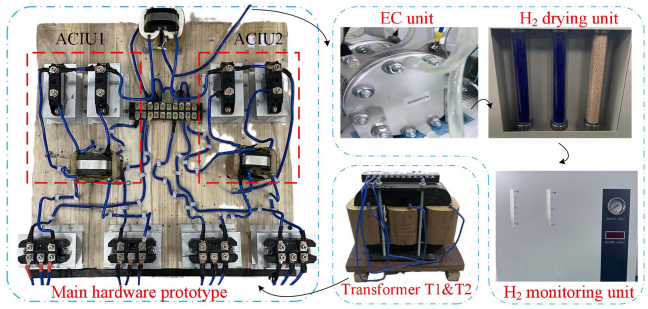

Fig. 6. Experimental setup of proposed hydrogen production power supply.

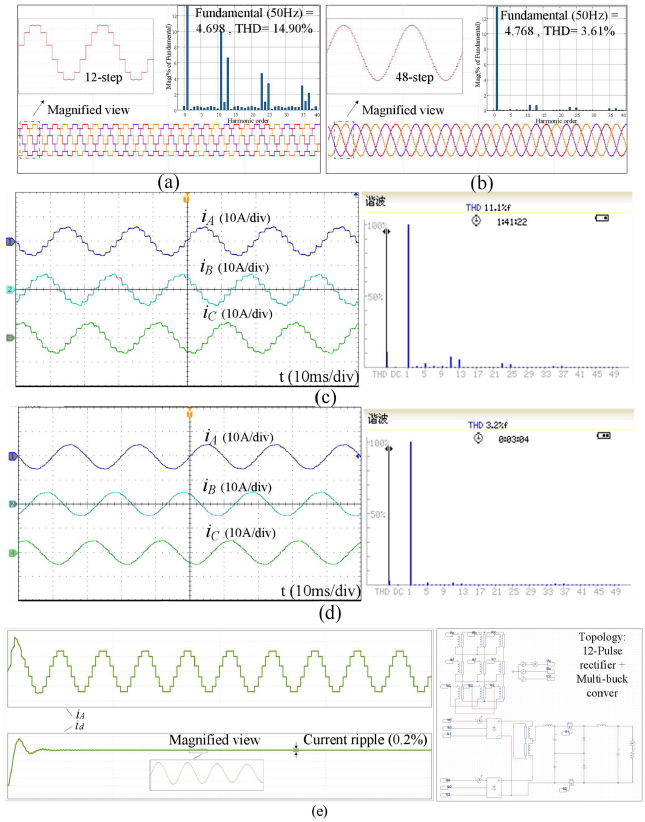

Fig. 7. Power quality analysis. (a) Simulation result of input current and THD without ACIU. (b) Simulation result of input current and THD with ACIU. (c) Experimental result of input current and THD without ACIU. (d) Experimental result of input current and THD ACIU. (e) Input and output current waveforms of 12-pulse diode rectifier with multibuck converter.

current and the THD of the rectifier, both with and without the ACIU. The simulation results are depicted in Fig. 7(a) and (b), showing that the proposed method achieves a highly effective 48-step waveform, significantly reducing the THD from 14.90% to 3.61%. In addition, the experimental results are presented in Fig. 7(c) and (d). Due to the influence of leakage inductance, the measured THD is slightly lower than the simulated values, and the input current demonstrates improved smoothness. Therefore, the proposed method exhibits strong harmonic suppression capabilities, achieving a measured THD of 3.2%. Also, the 12-pulse diode rectifier with the multibuck converter is simulated, and

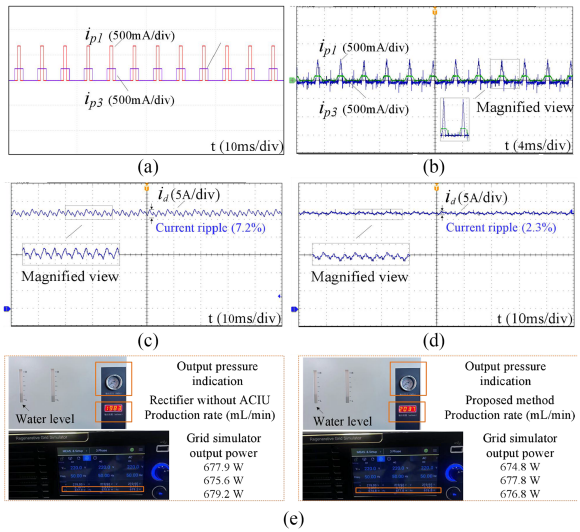

Fig. 8. Analysis of hydrogen production efficiency. (a) Simulation results of injection current i_{p1}&i_{p3}. (b) Experimental results of injection current i_{p1} and i_{p3}. (c) Experimental result of output current of rectifier without ACIU. (d) Experimental result of output current of proposed method. (e) Display of H2 meter of rectifier without ACIU and proposed method.

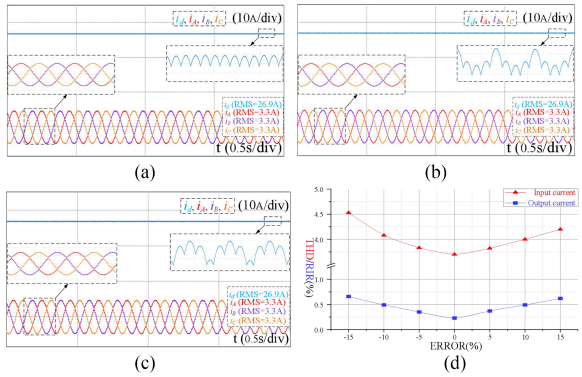

Fig. 9. Power performance analysis. (a) Simulation result of input current of proposed scheme. (b) Considering fault tolerance of +10% in ACIU. (c) Considering fault tolerance of −10% in ACIU. (d) Power quality under different fault-tolerant conditions.

the key waveforms are shown in Fig. 7(e). While the scheme effectively suppresses the current ripple, its inherent topology introduces significant harmonic distortion into the grid, necessitating supplementary passive/active filter for compliance with power quality standards. Furthermore, the direct conduction of high-amplitude currents through PWM converters imposes substantial thermal stress.

Second, the harmonic distortion in the proposed method is significantly minimized due to the implementation of the ACIU. Consequently, the waveform of the ACIU is presented. Fig. 8(a) and (b) shows the simulation and experimental waveforms of the currents i_{p1} and i_{p3}, respectively. It can be seen that the currents i_{p1} and i_{p3} became the square wave with a frequency of 150 Hz, and these are consistent with the simulation result. Meanwhile, due to the influence of leakage inductance, the rising and falling edges are presented in Fig. 8(b), and are gentler than those of the simulation results in Fig. 8(a). In both cases, the input power was kept constant to ensure that the observed increase in hydrogen production is attributed solely to the proposed method and not to differences in power input. Furthermore, Fig. 8(c)–(e) illustrates the output current i_d and the hydrogen production of the rectifier both with and without the ACIU. It is evident that the current ripple is reduced from 7.2% to 2.3%, while hydrogen production increases from 1983 to 2037 mL/min, accompanied by a 2.7% enhancement in efficiency. This is because the hydrogen production of the EC is directly proportional to the mean value of dc current supplied to the EC and the current ripple causes local overheating and additional losses in EC [3]. Furthermore, the high ripple can induce fluctuations in current density, resulting in nonuniform reactions on the electrode surface, which in turn accelerate electrode corrosion or lead to uneven deposition. This improvement highlights its suitability for hydrogen production applications.

Finally, the comprehensive performance assessments, including fault tolerance analysis, have been conducted. Fig. 9(a) illustrates the input and output current waveforms using the parameters derived from theoretical analysis within the ACIU. Fig. 9(b) depicts the input and output currents under a +10% fault tolerance in the ACIU. As a result, the THD of the input current increases from 3.7% to 4%, and the ripple of the output current rises from 0.23% to 0.49%. Similarly, as shown in Fig. 9(c), considering a −10% fault tolerance in the ACIU, the THD of the input current and the ripple of the output current increased to 4.1% and 0.5%, respectively. Furthermore, Fig. 9(d) presents the THD of the input current and the ripple of the output current under various levels of fault tolerance. As observed in Fig. 9(d), the proposed hydrogen production power supply consistently maintains high power quality.

VI. Conclusion

A novel rectifier specifically engineered for low-voltage and high-current applications presents innovative solutions for electrolytic hydrogen production. This study thoroughly analyzes the operational requirements, the design of ACIU and kVA rating. Both simulation and experimental results have been conducted to validate the theoretical analysis. The findings indicate that the ripple and harmonic distortions were effectively maintained below 2.5% and 3.5%, respectively. Furthermore, the fault tolerance characteristics enhance mass production capabilities, while the reduced costs render seamless power capacity expansion feasible.

References

[1] H. Tian, W. Han, M. Chen, G. Liang, and Z. Tang, "Common-ground type switching step-up/step-down VSI for grid-connected PV system," *IEEE Trans. Power Electron.*, vol. 39, no. 8, pp. 10390–10398, Aug. 2024, doi: 10.1109/TPEL.2024.3393624.

[2] H. Cheng, Y. Xia, and W. Wei, "Self-optimization control for alkaline water electrolyzers considering electrolyzer temperature variations," *IEEE Trans. Ind. Electron.*, vol. 72, no. 3, pp. 2700–2711, Mar. 2025, doi: 10.1109/TIE.2024.3440494.

[3] H. Tian, W. Han, J. Sathik M, M. Chen, G. Liang, and S. Mekhilef, "High-efficiency, High-power asymmetrically designed three-phase power supply for electrolytic hydrogen production," *IEEE Trans. Power Electron.*, vol. 40, no. 1, pp. 92–97, Jan. 2025, doi: 10.1109/TPEL.2024.3464675.

[4] J. Wang, A. Chen, L. Li, C. Zhao, X. Yao, and Q. Chen, "A simple 36-pulse rectifier with passive pulse-tripling circuit at the DC side," *IEEE Trans. Ind. Electron.*, vol. 70, no. 1, pp. 17–28, Jan. 2023, doi: 10.1109/TIE.2022.3150109.

[5] Q. Du, L. Gao, Q. Li, T. Li, and F. Meng, "Harmonic reduction methods at DC side of parallel-connected multipulse rectifiers: A review," *IEEE Trans. Power Electron.*, vol. 36, no. 3, pp. 2768–2782, Mar. 2021, doi: 10.1109/TPEL.2020.3013407.

[6] J. Wang, Y. Lv, L. Li, X. Yao, Q. Guan, and Q. Chen, "A 24-pulse rectifier with a passive auxiliary current injection circuit at DC side," *IEEE Trans. Power Electron.*, vol. 37, no. 9, pp. 11109–11123, Sep. 2022, doi: 10.1109/TPEL.2022.3160944.

[7] S. Yang, J. Wang, and W. Yang, "A novel 24-pulse diode rectifier with an auxiliary single-phase full-wave rectifier at DC side," *IEEE Trans. Power Electron.*, vol. 32, no. 3, pp. 1885–1893, Mar. 2017, doi: 10.1109/TPEL.2016.2560200.

[8] Y. Lian, S. Yang, and W. Yang, "Optimum design of 48-pulse rectifier using unconventional interphase reactor," *IEEE Access*, vol. 7, pp. 61240–61250, 2019, doi: 10.1109/ACCESS.2019.2902453.

[9] J. Chen, H. Bai, J. Chen, and C. Gong, "A novel parallel configured 48-pulse autotransformer rectifier for aviation application," *IEEE Trans. Power Electron.*, vol. 37, no. 2, pp. 2125–2138, Feb. 2022, doi: 10.1109/TPEL.2021.3106322.

[10] J. Wang, T. Liu, T. Yu, C. Zhao, X. Yao, and Q. Chen, "A series-connected 24-pulse star rectifier employing two different pulse-doubling interphase reactors," *IEEE Trans. Power Electron.*, vol. 39, no. 1, pp. 1460–1481, Jan. 2024, doi: 10.1109/TPEL.2023.3323795.

[11] Q. Li, F. Meng, L. Gao, H. Zhang, and Q. Du, "A 30-pulse rectifier using passive voltage harmonic injection method at DC link," *IEEE Trans. Ind. Electron.*, vol. 67, no. 11, pp. 9273–9291, Nov. 2020, doi: 10.1109/TIE.2019.2956404.

[12] Q. Du, L. Gao, Q. Li, S. Wang, F. Li, and F. Meng, "Research on the DC-side passive harmonic reduction methods of the ultramultiphase parallel-connected multipulse rectifier," *IEEE Trans. Power Electron.*, vol. 37, no. 12, pp. 14809–14819, Dec. 2022, doi: 10.1109/TPEL.2022.3197307.

[13] M. S. Akther, F. Afreen Nishat, M. M. Alam, R. Parvin Mou, and M. S. Ali, "A unique 48-pulse passive rectifier for harmonics compensation," in *Proc. IEEE Int. Women Eng. Conf. Elect. Comput. Eng.*, 2020, pp. 1–4, doi: 10.1109/WIECON-ECE52138.2020.9397937.

[14] T. Song, Y. Zhang, F. Gao, X. Zhu, J. Shan, and Z. Kong, "Power model free voltage ripple suppression method of three-phase PWM rectifier under unbalanced grid," *IEEE Trans. Power Electron.*, vol. 37, no. 11, pp. 13799–13807, Nov. 2022, doi: 10.1109/TPEL.2022.3184403.

[15] H. Ding, Q. Hu, J. Li, J. Lin, L. Hong, and Z. Wu, "An electrolyzer model for power system operation optimization over broad temperature range," *IEEE Trans. Sustain. Energy*, vol. 15, no. 3, pp. 2126–2129, Jul. 2024, doi: 10.1109/TSTE.2024.3375074.